

Article

Low Frequency Damping Control for Power Electronics-Based AC Grid Using Inverters with Built-In PSS

Ming Yang ¹, Wu Cao ^{1,*}, Tingjun Lin ¹, Jianfeng Zhao ¹ and Wei Li ²

- ¹ School of Electrical Engineering, Southeast University, Nanjing 210096, China; mingyang_ee@seu.edu.cn (M.Y.); 220192720@seu.edu.cn (T.L.); jianfeng_zhao@seu.edu.cn (J.Z.)
² NARI Group Corporation (State Grid Electric Power Research Institute), Nanjing 211106, China; liwei10@sgepri.sgcc.com.cn
* Correspondence: caowu_ee@seu.edu.cn

Abstract: Low frequency oscillations are the most easily occurring dynamic stability problem in the power system. With the increasing capacity of power electronic equipment, the coupling coordination of a synchronous generator and inverter in a low frequency range is worth to be studied further. This paper analyzes the mechanism of the interaction between a normal active/reactive power control grid-connected inverters and power regulation of a synchronous generator. Based on the mechanism, the power system stabilizer built in the inverter is used to increase damping in low frequency range. The small-signal model for electromagnetic torque interaction between the grid-connected inverters and the generator is analyzed first. The small-signal model is the basis for the inverters to provide damping with specific amplitude and phase. The additional damping torque control of the inverters is realized through a built-in power system stabilizer. The fundamentals and the structure of a built-in power system stabilizer are illustrated. The built-in power system stabilizer can be realized through the active or reactive power control loop. The parameter design method is also proposed. With the proposed model and suppression method, the inverters can provide a certain damping torque to improve system stability. Finally, detailed system damping simulation results of the universal step test verify that the analysis is valid and effective.

Keywords: low frequency damping; grid-connected inverter; power system stabilizer; power electronics-based AC power system



Citation: Yang, M.; Cao, W.; Lin, T.; Zhao, J.; Li, W. Low Frequency Damping Control for Power Electronics-Based AC Grid Using Inverters with Built-In PSS. *Energies* **2021**, *14*, 2435. <https://doi.org/10.3390/en14092435>

Academic Editor: Juri Belikov

Received: 22 March 2021
Accepted: 22 April 2021
Published: 24 April 2021

Publisher's Note: MDPI stays neutral with regard to jurisdictional claims in published maps and institutional affiliations.



Copyright: © 2021 by the authors. Licensee MDPI, Basel, Switzerland. This article is an open access article distributed under the terms and conditions of the Creative Commons Attribution (CC BY) license (<https://creativecommons.org/licenses/by/4.0/>).

1. Introduction

The power system has expanded and changed incessantly. There is a trend that conventional power systems are expected to be replaced by next-generation power systems. The grid-connected inverters are the crucial component that delivers renewable energy and energy storage to the grid. The grid-connected inverter should play a more critical role in the power system [1–6]. Due to the negative damping effect of the power system, the phenomenon of low frequency oscillations (LFOs) often occurs on the transmission lines with long distances, heavy loads or weak connections. The typical feature of low frequency oscillation is power swing and low frequency ranging between 0.1 and 2.5 Hz. The power regulation characteristic of inverter is different from that of synchronous generator. In the same power grid, the power regulation of inverters affects the swing characteristics of generator's power angle. Obviously, the research of the influence mechanism of inverter power regulation on generator torque, and the low frequency damping control is important for the system stability.

There have been many studies on the low frequency damping control. The power system stabilizer (PSS) in excitation system is used to generate the damping effect. The PSS suppresses LFOs through controlling electromagnetic torque variation. PSS in excitation system has been proved to be the most cost-effective damping control [7–10]. In power electronics-based AC grid, the proportion of synchronous generator capacity decreases.

The damping torque provided by the excitation system is not enough for LFOs suppression. Some power electronic devices such like unified power flow controller (UPFC), static var compensators (SVC), voltage source converter based high voltage direct current (VSC-HVDC) are researched to suppress the LFOs. The power electronic equipment can increase the system damping to inhibit oscillation [11–14]. References [15–19] analyze the impact of VSC control parameters on power system stability based on small-signal stability analysis. Reference [20] proposes a UPFC-based stabilizer that adopts a conventional PI controller and a lead-lag controller to produce the damping effect. Because of the UPFC covers active and reactive power controls with multiple time scales, the low frequency damping control parameters of UPFC are hard to design for most working condition. References [21,22] research the SVC with a damping controller. The damping control in SVC increases system damping by reactive power control. The influence of SVC's reactive power on generator is limited by distance and area. Reference [23–26] proposes VSC-HVDC damping strategies. These strategies are realized by adding angular velocity close loop control to the basic control of inverter. The damping control and the normal inverter control both regulate the active power. But the purpose of control is different. So, the two kinds of control are easy to affect each other, and the parameters are hard to design. For the situation that the virtual synchronous generator (VSG) control changes the regulation characteristic of inverter, references [27,28] investigates extra damping control in the VSG control. The damping capacity of inverter can not be fully utilized due to the limitation of virtual inertia control.

There are still some improvements as follows in the research of low frequency damping control in power electronic based AC grid.

(1) The capacity proportion of the UPFC and SVC is small in the power system. The damping effect of the UPFC and SVC is limited. The low frequency damping control should focus on the grid-connected inverters which have large proportion.

(2) These stability analyses mainly focus on the inverter itself. The correlation with generators in the power grid has not been considered enough. The influence of grid-connected inverter with normal active/reactive power control on the electromagnetic torque of the synchronous generator has little research. Using the mechanism of the influence to improve the dynamic safety and stability of the power system has not been fully considered.

(3) The different time scales controls are directly superimposed together in the inverters based on existing research. Without the detailed model for the interaction between inverters and generators, the control parameters are hard to set.

To improve the low frequency damping control and LFOs suppression, the main contributions of this paper are as follows:

(1) This paper investigates how grid-connected inverter with normal active/reactive power control influences the electromagnetic torque of the synchronous generator. The small-signal model for the impact of the output of the grid-connected inverter on the electromagnetic torque of the synchronous generator is proposed. The damping torque analysis is used to evaluate the effect of inverter on low frequency damping. The mechanism of grid-connected inverter providing positive damping is found. That can also be suitable for multi grid-connected inverters with same voltage and current control.

(2) The control time scale of the introduced damping control is adapted to the frequency range of LFOs. It is independent of the original fast control of the inverter. The method of introducing electromagnetic damping torque with built-in PSS to increase low frequency damping is proposed. The structure and parameter design method is also proposed. The additional electromagnetic damping control can be realized by the active power control or reactive power control of the inverter. Because of most of the inverters in power system output active power, the built-in PSS realized through the active power control are taken as the object of analysis. That is different from the excitation system's PSS. The difference between traditional PSS in excitation system and the proposed built-in PSS in inverter can be illustrated in Figure 1, where V_{ref} is the terminal voltage control reference value for excitation system, V_t is the terminal voltage value, E_{fd} is the excitation voltage,

P_{ref} is the active power control reference value for inverter, P is the active power actual value, Q_{ref} is the reactive power control reference value for inverter, Q is the reactive power actual value, $G_{i-P}(s)$ is the active power control, $G_{i-Q}(s)$ is the reactive power control, $G(s)$ is the excitation control.

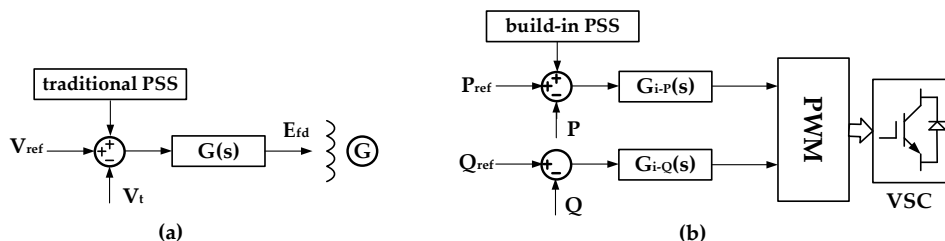


Figure 1. Traditional PSS in excitation system and the proposed built-in PSS in inverter. (a) Traditional PSS in excitation system; (b) the proposed built-in PSS in inverter.

(3) To verify the above analysis, two-part simulation is used. One part is about different damping torques' effect on single grid-connected inverter. The different damping torques are realized by using different parameters. The other part is about the effectiveness of the built-in PSS for dual paralleled grid-connected inverters.

The rest of this paper is organized as follows. Section 2 derives a small-signal model of the impact of the grid-connected inverter on electromagnetic torque of synchronous generator. The influence of inverter output on damping torque is analyzed. Section 3 provides a design for built-in PSS based on the small signal model. Section 4 gives the simulation result. The conclusions of this paper are presented in Section 5.

2. Modeling and Analysis

The study of the generator oscillation process shows that in most cases the generator rotor oscillation is related to the mechanical inertia time constant. The electrical angular velocity ($\Delta\omega$) and electrical acceleration ($\Delta\delta$) are used to describe the oscillations. The mechanical inertia time constant represents lower oscillation frequency and slower attenuation [29]. So, in the study of the process related to rotor oscillation, the fast process can be considered to be over. In the process of modelling, circuit impedance could be calculated under the situation of the rated frequency of power grid.

The electromagnetic torque of synchronous generator is used to increase low frequency damping because of its fast-changing characteristics. The power regulation of the grid-connected inverters affects the electromagnetic torque of synchronous generator. So, the influence of electromagnetic torque caused by inverter power regulation is the first problem to be clarified.

2.1. System Description

Figure 2 depicts the structure of a typical structure of power electronics-based AC power system. The power electronics-based AC power system has synchronous generators and multi inverters. The inverters have a considerable proportion of the transformation and consumption capacity in power grid. The normal control architecture of the inverter controller is shown in Figure 3, where P_{ref} is the d-axis control reference of active power, U_{dcref} is the d-axis control reference of DC voltage, Q_{ref} is the q-axis control reference of reactive power, U_{acref} is the q-axis control reference of AC voltage, i_{2dref} is the d-axis reference current value of inverter, i_{2qref} is the q-axis reference current value of inverter, i_{2d} is the d-axis current value of inverter, i_{2q} is the q-axis current value of inverter, U_{cd} is the d-axis component of system side voltage, U_{cq} is the q-axis component of system side voltage, Δv_d is the d-axis component variation of inverter side voltage, Δv_q is the q-axis component variation of inverter side voltage. $F_o(s)$ is the outer-loop control function of the inverter, $F(s)$ is the inner-loop control function of the inverter.

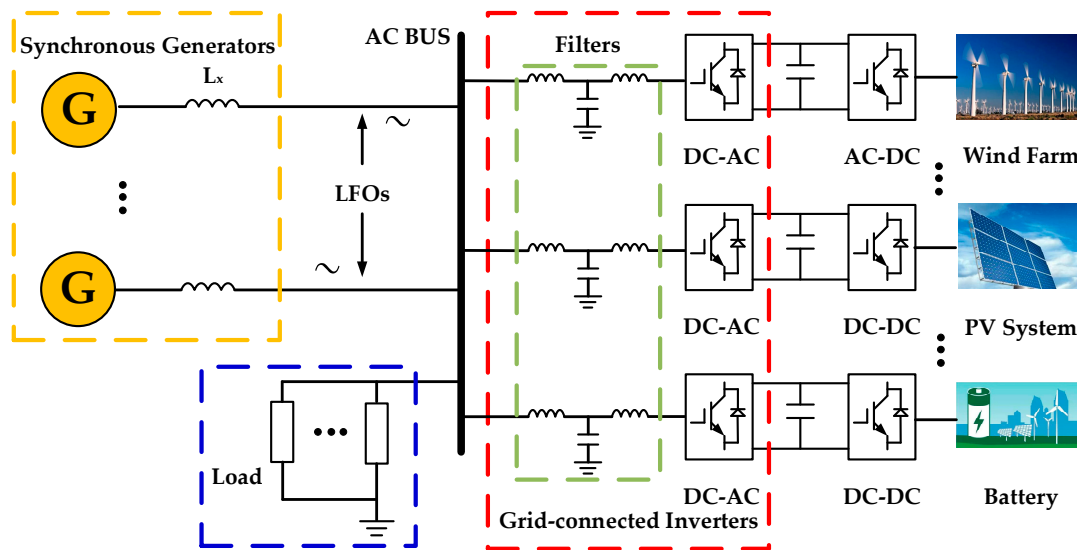


Figure 2. A typical set up of power electronics-based AC power system.

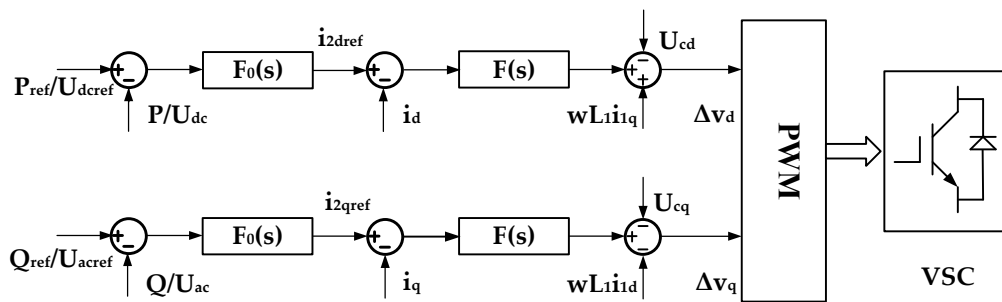


Figure 3. The typical control structure of the inverter.

The multi-inverters shown in Figure 2 can be considered as a controllable voltage source, connecting to the power grid with an LCL filter typically. The multi generators can be equivalent as a voltage source with characteristics of synchronous generator. Figure 4 is the equivalent two-port network of the system shown in Figure 2, where U is the voltage of the generator, V is the voltage of the inverter, x_s is the contact inductive reactance, x_0 is the inductive reactance of load, r is the resistance of the load, x_1 and x_2 is the inductive reactance of LCL filter for the inverter and y_c is the admittance of LCL filter for the inverter.

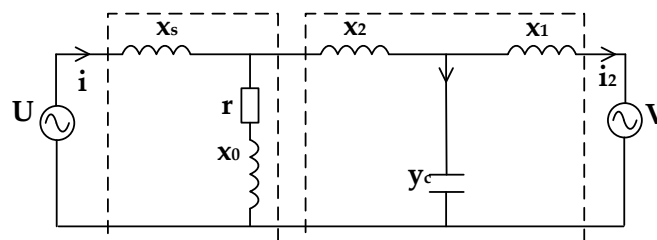


Figure 4. Two-port network for simplified power electronics-based AC power system.

The loop circuit equation of two-port network is shown in the following:

$$\begin{pmatrix} u \\ i \end{pmatrix} = \begin{pmatrix} z_{11}z'_{22} + z_{12}z'_{32} & z_{11}z'_{23} + z_{12}z'_{33} \\ z_{21}z'_{22} + z_{22}z'_{32} & z_{21}z'_{23} + z_{22}z'_{33} \end{pmatrix} \begin{pmatrix} v \\ i_2 \end{pmatrix} \quad (1)$$

where $z_{11}, z_{12}, z_{21}, z_{22}$ and $z'_{22}, z'_{23}, z'_{32}, z'_{33}$ are the impedance of two-port networks 1 and 2, respectively, i and i_2 are the currents of the line connected with the generator and the inverter, respectively.

Then, the current of the generator in dq synchronous frame is got as:

$$\begin{cases} i_d = y_1 u_d + y_2 u_q + y_3 v_d + y_4 v_q \\ i_q = y_5 u_d + y_6 u_q + y_7 v_d + y_8 v_q \end{cases} \quad (2)$$

where $y_1 \sim y_6$ represents the correlation impedance, v_d is the d-axis component of inverter side voltage, v_q is the q-axis component of inverter side voltage, u_d is the d-axis voltage of the generator, u_q is the q-axis voltage of generator.

2.2. System Modeling

Through Equation (2), the small-signal model of generator's current and voltage is derived as shown in Equation (3).

$$\begin{cases} \Delta u_d = x_q \Delta i_q \\ \Delta u_q = \Delta E'_q - x'_d \Delta i_d \\ \Delta i_d = y_1 \Delta u_d + y_2 \Delta u_q + y_3 \Delta v_d + y_4 \Delta v_q \\ \Delta i_q = y_5 \Delta u_d + y_6 \Delta u_q + y_7 \Delta v_d + y_8 \Delta v_q \end{cases} \quad (3)$$

where x'_d is the d-axis transient resistance of the generator, x_q is the q-axis resistance of the generator, i_d is the d-axis current of the generator, i_q is the q-axis current of generator, u_d is the d-axis voltage of the generator, u_q is the q-axis voltage of generator, E_q is the internal potential of the generator, Δ represents the micro change of electrical quantities.

The expression of Δi_d and Δi_q could be derived by eliminating Δu_d and Δu_q and illustrated as Equation (4):

$$\begin{cases} \Delta i_d = Z_1 \Delta E'_q + Z_2 \Delta v_d + Z_3 \Delta v_q \\ \Delta i_q = Z_4 \Delta E'_q + Z_5 \Delta v_d + Z_6 \Delta v_q \end{cases} \quad (4)$$

where $Z_1 \sim Z_6$ are the admittance coefficient which are derived through Equation (3).

A series equation of electromagnetic relation of the generator is shown as the following Equation (5) [7]:

$$\begin{cases} u_d = x_q i_q \\ u_q = E_q - (x_d - x'_d) i_d = E'_q - x'_d i_d \\ M_e = u_d i_d + u_q i_q = E_Q i_q \\ E'_q = E_Q - (x_q - x'_d) i_d \\ \frac{dE'_q}{dt} = \frac{1}{T'_{d0}} (E_{fd} - E_q) \\ u^2 = u_d^2 + u_q^2 \end{cases} \quad (5)$$

where E'_q is a hypothetical potential which is proportional to the flux of excitation system, M_e is the electromagnetic torque of the generator, E_Q is hypothetical potential behind x_q , E_{fd} is the excitation voltage, T'_{d0} is the time constant of the rotor when the stator is open-circuit.

The small-signal model of the generator is derived as:

$$\begin{cases} \Delta M_e = i_{q0} \Delta E'_q + i_{q0} (x_q - x'_d) \Delta i_d + E_{Q0} \Delta i_q \\ (1 + T'_{d0} s) \Delta E'_q = \Delta E_{fd} - (x_q - x'_d) \Delta i_d \\ \Delta u = \frac{u_{d0}}{u_0} x_q \Delta i_q + \frac{u_{q0}}{u_0} (\Delta E'_q - x'_d \Delta i_d) \end{cases} \quad (6)$$

where i_{q0} is the steady-state q-axis current of the generator, u_{d0} is the steady-state d-axis voltage of the generator, u_{q0} is the steady-state q-axis voltage of the generator, u_0 is the steady-state voltage of the generator, E_{Q0} is the hypothetical steady-state potential behind x_q .

The small-signal model of the synchronous generator with inverter’s voltage is derived in Equation (7) by substituting Equation (4) of Δi_d and Δi_q into Equation (6).

$$\begin{cases} \Delta M_e = K_1 \Delta E'_q + K_2 \Delta v_d + K_3 \Delta v_q \\ \Delta E'_q = K_4 \Delta E_{fd} - K_5 \Delta v_d - K_6 \Delta v_q \\ \Delta u = K_7 \Delta E'_q + K_8 \Delta v_d + K_9 \Delta v_q \\ \Delta E_{fd} = G(s) \Delta u \end{cases} \begin{cases} K_1 = i_{q0} + i_{q0}(x_q - x'_d)Z_1 - E_{Q0}Z_4 \\ K_2 = i_{q0}(x_q - x'_d)Z_2 + E_{Q0}Z_5 \\ K_3 = i_{q0}(x_q - x'_d)Z_3 + E_{Q0}Z_6 \end{cases} \quad (7)$$

$$\begin{cases} K_4 = \frac{1}{1 + (x_q - x'_d)Z_1 + T'_{d0}s} \\ K_5 = K_4(x_q - x'_d)Z_2 \\ K_6 = K_4(x_q - x'_d)Z_3 \end{cases} \begin{cases} K_7 = \frac{u_{d0}}{u_0} x_q Z_4 + \frac{u_{q0}}{u_0} - \frac{u_{q0}}{u_0} x'_d Z_1 \\ K_8 = \frac{u_{d0}}{u_0} x_q Z_5 - \frac{u_{q0}}{u_0} x'_d Z_2 \\ K_9 = \frac{u_{d0}}{u_0} x_q Z_6 - \frac{u_{q0}}{u_0} x'_d Z_3 \end{cases}$$

$G(s)$ represents the transfer function of the excitation system.

Consider the inverter control shown in Figure 3, the block diagram of the small-signal control model of the generator-inverter system can be obtained from the above analysis as Figure 5.

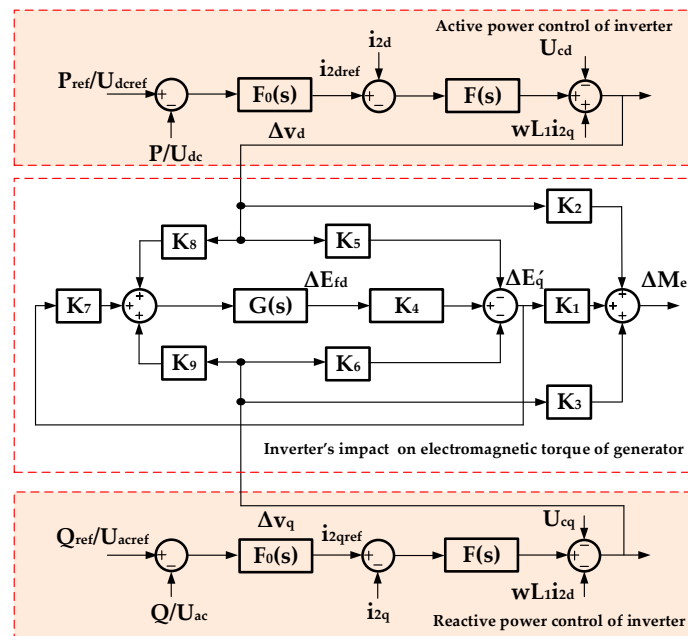


Figure 5. The small-signal model of the inverter output and the generator electromagnetic torque.

According to the control block diagram and the superposition principle, the transfer functions of $\Delta M_e / \Delta V_d$ and $\Delta M_e / \Delta V_q$ are obtained, respectively:

$$\begin{cases} \frac{\Delta M_e}{\Delta v_d} = \frac{(K_1 K_8 - K_2 K_7) G K_4 - K_1 K_5 + K_2}{1 - K_7 G K_4} \\ \frac{\Delta M_e}{\Delta v_q} = \frac{(K_1 K_9 - K_3 K_7) G K_4 - K_1 K_6 + K_3}{1 - K_7 G K_4} \\ G(s) = \frac{k_i + k_p s}{s} \end{cases} \quad (8)$$

where k_i is the integral time constant, k_p is the proportion coefficient.

The phase and amplitude difference between the output of the grid-connect inverter and the electromagnetic torque of the synchronous generator can be calculated by Equation (8). In this chapter, the small-signal model of the impact of the grid-connected inverter on electromagnetic torque of synchronous generator in power electronics-based AC power system has been deduced. The model reveals the relationship between the output power of the inverter and the generator torque. The model is the analysis basis of using the grid-connected inverter to increase low frequency damping.

According to the classical power system theory, a torque can be decomposed into two components, i.e., damping torque and synchronizing torque. The positive direction of the damping torque is in phase with the angular frequency $\Delta\omega$. The positive direction of the synchronizing torque is in phase with the angle $\Delta\delta$. The influence of normal control grid-connected inverter on low frequency damping mainly depends on the $\Delta\omega$ direction component of electromagnetic torque.

According to the Heffron-Philips model, the relationship between terminal voltage and power angle can be present as Equation (9).

$$\begin{cases} \Delta u = K_{5H-P}\Delta\delta + K_{6H-P}\Delta E'_q \\ K_{5H-P} = \frac{u_{d0}}{u_0} \frac{x_q}{x_q+x_l} U_L \cos \delta_0 - \frac{u_{q0}}{u_0} \frac{x'_d}{x'_d+x_l} U_L \sin \delta_0 \\ K_{6H-P} = \frac{u_{q0}}{u_0} \frac{x_l}{x'_d+x_l} \end{cases} \quad (9)$$

where $\Delta\delta$ is the power angle deviation, K_{5H-P} is the factor of $\Delta\delta$ in the Heffron-Philips model, K_{6H-P} is the factor of $\Delta E'_q$ in Heffron-Philips model, x_l is the line impedance and U_L is the voltage behind line impedance x_l .

According to Equation (9), Δu occurs when there is a disturbance of power angle. The variation of the active power of grid-connect inverter ΔP can be assumed to follow Δu . Moreover, the regulation of active power in the inverter is in the opposite direction of active power measurement variation. After a series of PI control, the phase of ΔM_e produced by grid-connect inverter lags the phase of $-\Delta u$. So, the torque phasor diagram under oscillation can be shown in Figure 6, where Δu is the component related to power angle, ΔM_{eD} is the damping torque component of ΔM_e , ΔM_{eS} is the synchronizing torque component of ΔM_e , θ_M represents the phase difference from the phase of $-\Delta u$ to the phase of ΔM_e . From Figure 6, it can be seen that the damping torque component of ΔM_e is negative. The negative damping reduces the damping of the system and makes it easier for the appearance of LFOs.

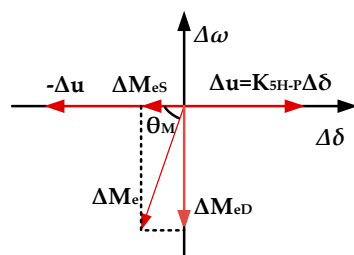


Figure 6. Torque phasor diagram during oscillation.

3. LFOs Suppression Strategy Using Inverter with Built-In PSS

3.1. The Control Structure of the Inverte with Built-In PSS

In order to increase low frequency damping, the grid-connected inverter needs to increase the torque in the positive direction of the axis $\Delta\omega$ to increase the damping torque. An extra torque ΔT can be introduced to provide positive synchronizing torque in the frequency range of LFOs. From Figure 4 and Equation (8), an additional control that passes the lead-lag correction component and inverter control loop can be introduced into the control loop of the grid-connected inverter to make the inverter produce positive damping torque.

To introduce the positive direction of the axis $\Delta\omega$, the active power or electric angular velocity on the interconnection line can be taken as the input of the additional control. Active power or angular velocity signal is introduced into the grid-connected inverter to produce positive damping, which is similar to the purpose of installing PSS on the excitation system. So, the additional control in the grid-connected inverter can use the experience of the structure of PSS to restrain LFOs. The grid-connected inverter is not willing to produce additional torque due to the normal power regulation of the generator, which will affect

its output capacity. Regarding the control structure of PSS2B, the acceleration power is used as the input signal. After the acceleration power input signal passes through a series of lead-lag components, the output phase is corrected to produce positive damping to suppress LFOs.

The built-in PSS structure for grid-connected inverter and application in the system is shown in Figure 7, where P_{ref} is the d-axis control reference of active power, U_{dcref} is the d-axis control reference of DC voltage, Q_{ref} is the q-axis control reference of reactive power, U_{acref} is the q-axis control reference of AC voltage. ω and P_e is the input signal, T_{W1} is the time constant of the first DC block for input signal ω , T_{W2} is the time constant of the second DC block of input signal ω , T_{W3} is the time constant of the first DC block of input signal P_e , T_{W4} is the time constant of the second DC block for input signal P_e , K_{S2} is the gain coefficient of the integral component for input signal P_e , K_{S3} is a composite coefficient, T_6 is the time constant of the integral component for input signal P_e , K_{S1} is gain coefficient of regulating component, T_1 is the lead time constant of first lead-lag component, T_2 is the lead time constant of first lead-lag component, T_3 is the lead time constant of second lead-lag component, T_4 is the lag time constant of second lead-lag component, V_{BPSS} is the output of PSS for grid-connected inverter, V_{BPSS_max} is the upper limit of V_{BPSS} , V_{BPSS_min} is the lower limit of V_{BPSS} . V_{BPSS} is superimposed on the control target of the grid-connected inverter.

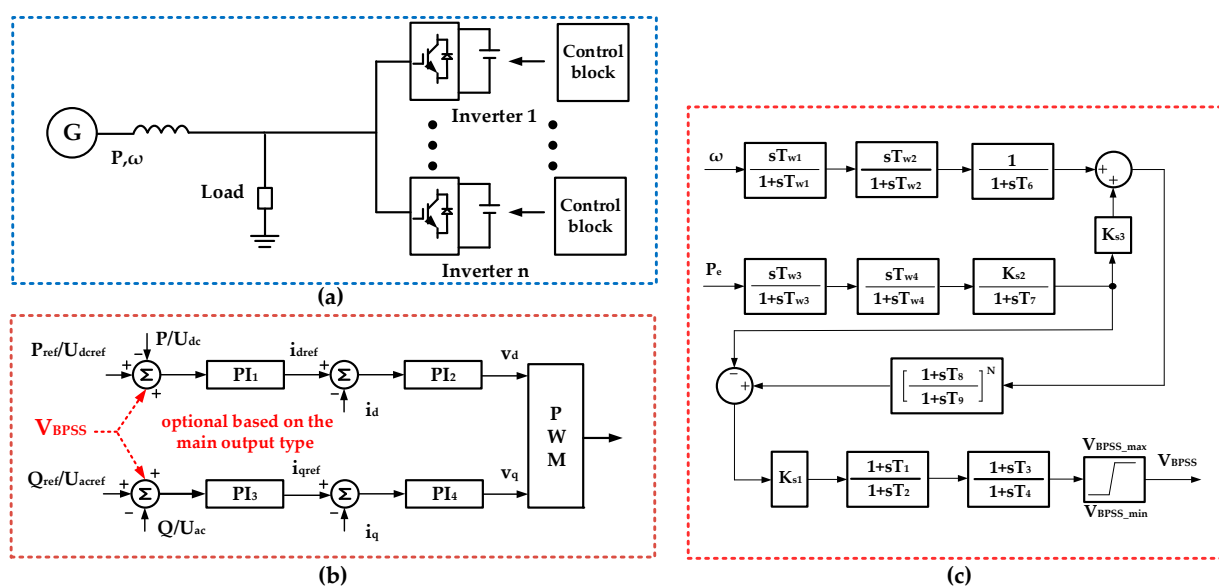


Figure 7. PSS control structure for grid-connected inverter and application in the system. (a) System structure; (b) superposition point of PSS output in the inverter control; (c) PSS control structure.

The additional electromagnetic torque is realized through the output of built-in PSS. The output of built-in PSS can be added with the reference of active power or reactive power in the control of grid-connected inverter. The superposition position is shown in Figure 7b, where The P_{ref}/U_{dcref} or Q_{ref}/U_{acref} in Figure 7b can be selected as the superimposed point according to the actual needs. When the grid-connected inverter output mainly active power, the built-in PSS shall be superposed on the corresponding active power control loop. When the grid-connected inverter output mainly reactive power, the built-in PSS shall be superposed on the corresponding reactive power control loop. The inverter damping torque control realized through active power control is different from the damping control of PSS realized through reactive power control of the generator.

3.2. Parameters Design Guideline for Built-In PSS

Different introduced extra torques have different damping effect. The angle between extra torque ΔT and $\Delta\omega$ axis and the amplitude of ΔT are the main factor determining damping torque. For the parameter tuning of built-in PSS, the lead-lag component parameters mainly determine the angle and K_{s1} determines the amplitude.

Undamped natural oscillation angular velocity is taken as the compensation point. The phase which the additional torque generated by built-in PSS lag to the input of the lead-lag components can be calculated through Equation (8). Then the parameters of the lead-lag components can be set according to the phase compensation demand. The other parameters of the filters in built-in PSS can use the design method of PSS which is used in excitation system.

As illustrated above, built-in PSS is superimposed on the reference of the outer-loop control. The additional control torque of built-in PSS has passed the control function $F_o(s)$ and $F(s)$. Then, the whole transfer function of additional torque of built-in PSS to electromagnetic torque of generator is shown as Equation (10).

$$\begin{cases} \frac{\Delta M_e}{\Delta\omega_{iPSS}} = \frac{\Delta M_e}{\Delta v_d} \cdot F_o(s) \cdot F(s) \\ F_o(s) = k_{po} + k_{io}/s \\ F(s) = k_{pi} + k_{ii}/s \end{cases} \quad (10)$$

where k_{po} is the proportion coefficient of the outer-loop control, k_{io} is the integral time constant of the outer-loop control, k_{pi} is the proportion coefficient of the inner-loop control, k_{ii} is the integral time constant of the inner-loop control.

According to the Heffron-Philips model, the undamped mechanical nature angular velocity of the rotor can be obtained through Equation (11).

$$\begin{cases} \omega_n = \sqrt{K_{1H-P}\omega_0/T_J} \\ K_{1H-P} = \frac{x_q - x_d'}{x_d' + x_s} i_{q0} u \sin \delta_0 + \frac{u \cos \delta_0}{x_q + x_s} E_{Q0} \end{cases} \quad (11)$$

where ω_n is the undamped mechanical nature angular velocity of the rotor, Δ_0 is the steady value of generator power-angle, ω_0 is the rated angular velocity, and T_J is the inertia constant of the generator.

When ω_n has been calculated, the phase of the whole system at the undamped mechanical nature angular velocity can be obtained through Equation (11). In order to produce positive damping torque and synchronous torque, the phase of additional damping torque should lead $\Delta\omega$ with phase 0~40 degrees. Then, compensatory angle ϕ_x of the lead-lag component of built-in PSS can be deduced.

The two lead-lag components of built-in PSS can adopt the same parameters. Then, T_1 is equal to T_3 , T_2 is equal to T_4 . As the inverter regulars very fast, the lag time constant T_2 is required to correspond with the speed. So, T_2 can be determined by reference to the regular time of inverter. The value of T_1 can be obtained according to the requirement of compensatory angle ϕ_x through Equation (12) as follow.

$$\phi_x/2 = \arctan T_1 \omega_n - \arctan T_2 \omega_n \quad (12)$$

When lead-lag component parameters are determined, K_{s1} can be determined by the critical gain method. The equivalent amplification factor of built-in PSS can be defined as AP, and its calculation formula is shown as Equation (13).

$$AP = K_{s1} \sqrt{\frac{1 + T_1^2}{1 + T_2^2}} \quad (13)$$

4. Verification

The classic step test of the generator terminal voltage is used to test low frequency damping. 5% step test of the generator terminal voltage is used in simulation and 3% step test of the generator terminal voltage is used in experiment. The damping effect of the built-in PSS can be observed in the process of the oscillation. The built-in PSS is a control for damping torque. So, the damping mechanism for multi-inverters with built-in PSS is same with the single inverter with built-in PSS. The simulation includes two parts. One part is about the different damping effects of different parameters of the built-in PSS. The other part is about the damping effects of dual paralleled grid-connected inverters with different built-in PSS situations. The experiment of generator-inverter system is also carried out to verify the damping control effect of the built-in PSS. The oscillation waveforms with and without built-in PSS in setting conditions are compared. The inverter can produce corresponding power oscillation which suppress the transmission power oscillation. The correctness of the analysis above is verified by the simulation and experimental result.

4.1. System Description and Setting

Simulation results based on PSCAD are provided to verify the analysis of built-in PSS. The simulation and experimental set up of a simplified power electronics-based AC power system is established as Figure 8. The two simulation parts uses single inverter and two paralleled inverters, respectively. The part with one inverter is used to verify the damping effects with different built-in PSS parameters. The part with two inverters is used to verify the damping effect of multi-inverters. The main parameters are shown in Table 1. The voltage of DC source is set as 400 V.

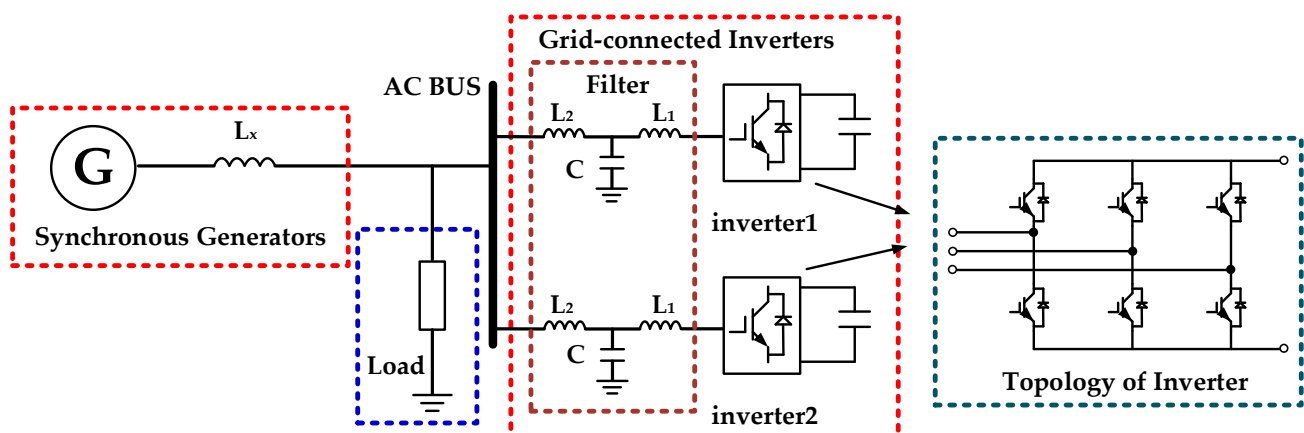


Figure 8. Simulation and experimental set up on PSCAD.

Table 1. Main parameters for simplified power electronics-based AC power system.

Parameters		Values
system impedance	L_s	0.1 mH
load	r	0.082 Ω
	L_0	0.082 mH
DC source	V_{dc}	400 V

Table 1. Cont.

	Parameters	Values
Generator	x'_d	0.0361 Ω
	x_q	0.2238 Ω
	T'_{d0}	3.55
	i_{d0}	1093.7 A
	i_{q0}	1803.7 A
	u_{d0}	285.6726 V
	u_{q0}	117.17 V
	u_0	308.77 V
	E_{Q0}	361.96 V
	S_{base}	1 MVA
	U_{tbase}	20 kV
excitation system control	k_p	100
	k_i	60
LCL filter	L_1	0.2 mH
	L_2	0.04 mH
	C	15 μ F
Inverter control F_0 (s)	k_{po}	4
	k_{io}	20
Inverter control F(s)	k_{pi}	4
	k_{ii}	100

4.2. Parameters Design

To make $T_1 \sim T_4$ positive, the output of built-in PSS is multiplied by -1 before adding to the reference value of active power control in this simulation, which results in a phase shift of 180° . According to the parameters of circuit and control function, the phase of ΔM_e lags the phase of $\Delta \omega_{BPSS}$ about $0 \sim 90^\circ$ in the frequency range of LFOs.

The output of built-in PSS is added with the output of d-axis control. The P_{ref} and Q_{ref} of the grid-connected inverter are set to be 0.4 MW and 0 MVar. According to the parameters of circuit and control function, ω_n can be calculated as 11.04 rad/s. From Figure 9 the phase of $\Delta M_e / \Delta \omega_{BPSS}$ at ω_n can be got as 75.1° .

Achieving $\Delta \omega_{BPSS}$ leading ΔM_e with 30° , this paper set compensatory angle ϕ_x of the lead-lag component of built-in PSS as 75° . According to the regulation time of the inverter, 0.01 can be taken as T_2 value. T_1 value can be derived through Equation (12). The parameters of built-in PSS are shown in Table 2. For see more details of the influence of built-in PSS, the limited output of built-in PSS is set quite lager as 20% of P_{ref} . In the actual project, the limit value should be according to the capacity of the inverter.

The bode diagram of $\Delta M_e / \Delta \omega_{BPSS}$ with and without compensation is shown in Figure 9. From the bode diagram, $\Delta \omega_{BPSS}$ leads ΔM_e 30 degree at the target frequency of LFOs. As the $\Delta \omega$ relevance vector is used as input, the phase of additional torque is 30 degrees lead of $\Delta \omega$ axis.

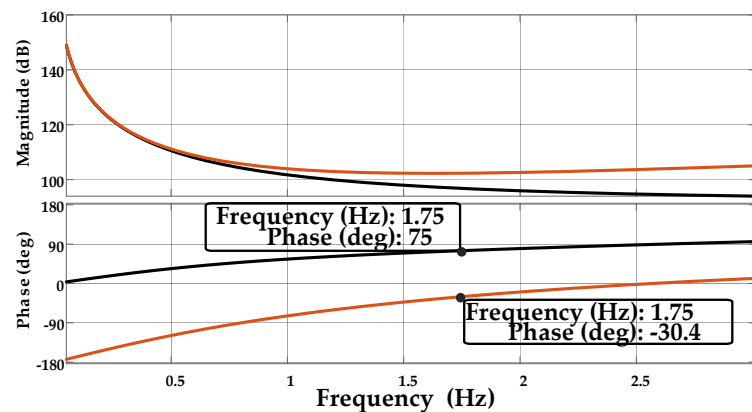


Figure 9. The bode diagram of $\Delta M_e/\Delta\omega_{BPSS}$ with and without compensation.

Table 2. Parameters of built-in PSS of inverter.

T_{w1}	T_{w2}	T_{w3}	T_{w4}	T_6	T_7	M
2	2	2	2	0	10	5
N	K_{s2}	K_{s3}	T_8	T_9	T_1	T_2
1	3.2	1	0.2	0.05	0.0868	0.01
T_3	T_4	K_{s1}	V_{BPSS_max}	V_{BPSS_max}		
0.0868	0.01	7.98	0.08 MW	−0.08 MW		

4.3. Damping Effects of Single Grid-Connected Inverter with Different Parameters

Case I is the situation that damping torques have same ϕ_x with different AP. Case II is the situation that damping torques have same AP with different ϕ_x . The simulation results are shown in Figure 10.

In case I compensatory angle ϕ_x of lead-lag component of built-in PSS is fixed as 75° , the damping torque diagram with different AP is shown in Figure 10a, where T_{BPSS0} is the damping torque of built-in PSS without phase compensation, T_{BPSS1} is the damping torque when $K_{s1} = 7.98$, T_{BPSS2} is the damping torque when $K_{s1} = 6$, T_{BPSS3} is the damping torque when $K_{s1} = 4$.

In case II AP of built-in PSS is fixed as 8.04, the damping torque diagram with different ϕ_x is shown in Figure 10a. Where T_{BPSS0} is the damping torque of built-in PSS without phase compensation, T_{BPSS1} is the damping torque when $\phi_x = 65^\circ$, T_{BPSS2} is the damping torque when $\phi_x = 75^\circ$, T_{BPSS3} is the damping torque when $\phi_x = 85^\circ$. Figure 10b shows the active power of generator in both cases; Figure 10c shows output of built-in PSS with various ϕ_x and AP; Figure 10d shows active power of grid-connected inverter in both cases; Figure 10e shows reactive power of grid-connected inverter in both cases; Figure 10f shows terminal voltage of generator in both cases.

For case I, from Figure 10b it can be seen that the bigger AP could produce larger positive damping torque. For case II, from Figure 10b the closer to the $\Delta\omega$ -axis could produce a larger positive damping torque. From Figure 10c,d it can be seen that larger output of the built-in PSS corresponds larger power fluctuation of inverter and larger positive damping torque. With the appropriate setting of K_{s1} and ϕ_x , the system damping can be increased. Under the action of built-in PSS, the active power fluctuation of inverter provides positive damping to the system. The verification results are consistent with the above theoretical analysis. Meanwhile, from Figure 10e,f, the damping regulation has little influence on terminal voltage of generator. The reason for that is that the built-in PSS in inverter is added to the active power control and the inverter adopts active and reactive power decoupling control strategy.

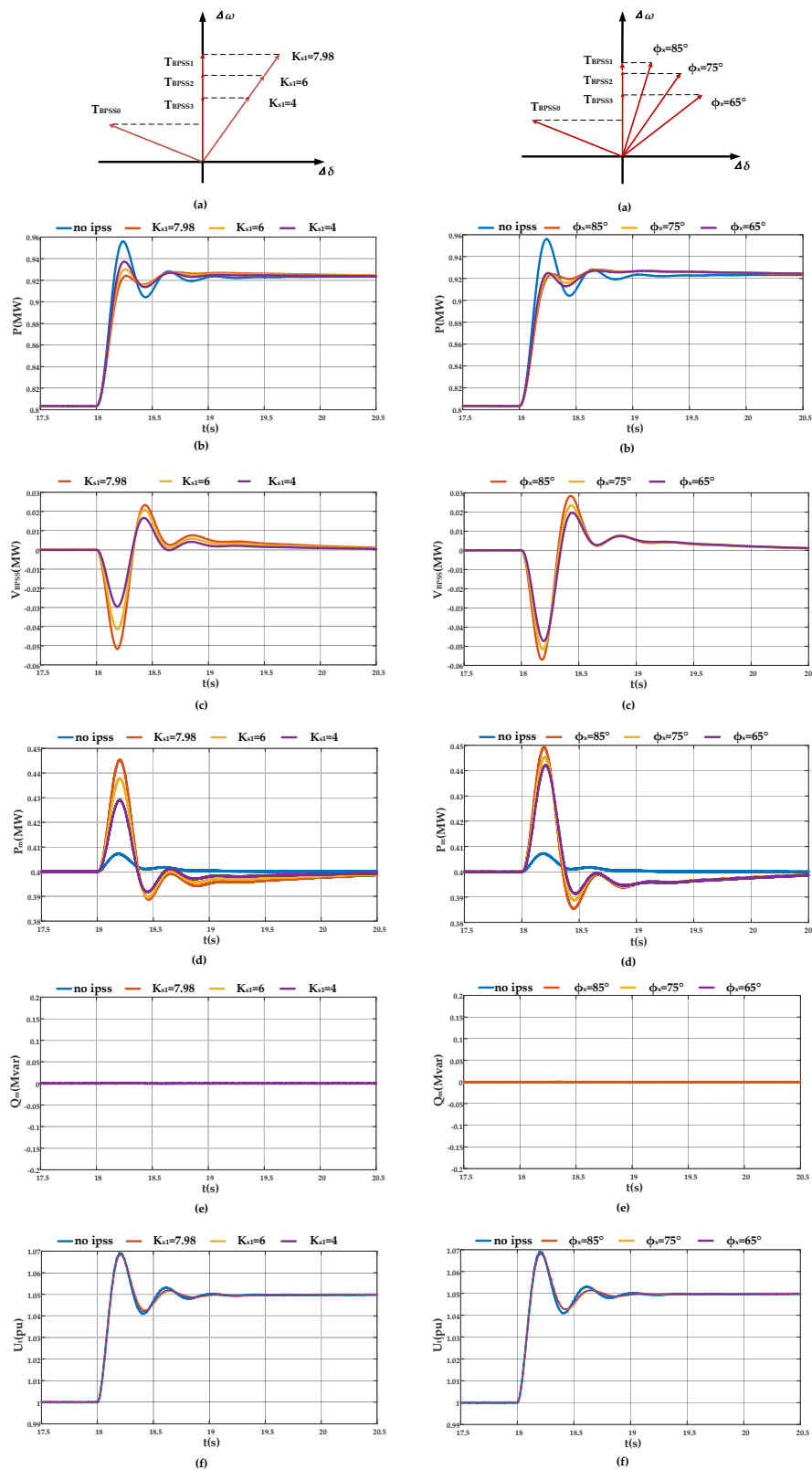


Figure 10. Simulation results of same ϕ_x with different AP (case I), same AP with different ϕ_x (case II). (a) Schematic diagram of damping torque with different AP and ϕ_x ; (b) active power of generator; (c) output of built-in PSS with various ϕ_x and AP; (d) active power of grid-connected inverter; (e) reactive power of grid-connected inverter; (f) terminal voltage of generator.

4.4. Damping Effects of Dual Paralleled Grid-Connected Inverters

More capacity of inverters to influence the electromagnetic torque of generator can present more damping effect. In this paper the situation of two inverters is taken as an example of multi-inverters connected with synchronous generator.

When the load is fixed, the different numbers of grid-connected inverters is set to realize the different distribution of active power between the inverter and the generator in the system shown in Figure 8. Figure 11 is the simulation result of two parallel grid-connected inverters system with different built-in PSS situations. The P_{ref} of the grid-connected inverter are set to be 0.4 MW and 0.2 MW, respectively. The Q_{ref} of the grid-connected inverter are set to be 0 MVar. The built-in PSS in both inverters adopts $K_{s1} = 6$ and same value as shown in Table 2 for the other parameters.

Three built-in PSS situations are simulated, case I: none of the inverters has built-in PSS; case II: only the larger output inverter has built-in PSS; case III: both of the inverters have built-in PSS. Figure 11a shows the fluctuation comparison of generator's active power under the three cases. From the figure it can be seen that better damping effect can be get by more inverters with built-in PSS. Figure 11b shows the active power of the larger output inverter under the three cases. Figure 11c shows the active power of the lower output inverter under the three cases. Figure 11d shows the output of built-in PSS in the inverters under the three cases. From Figure 11b–d, the active power fluctuation of the larger inverter can be reduced when two inverters have damping effect. The increasing of low frequency damping reduces the output of the built-in PSS of the inverter.

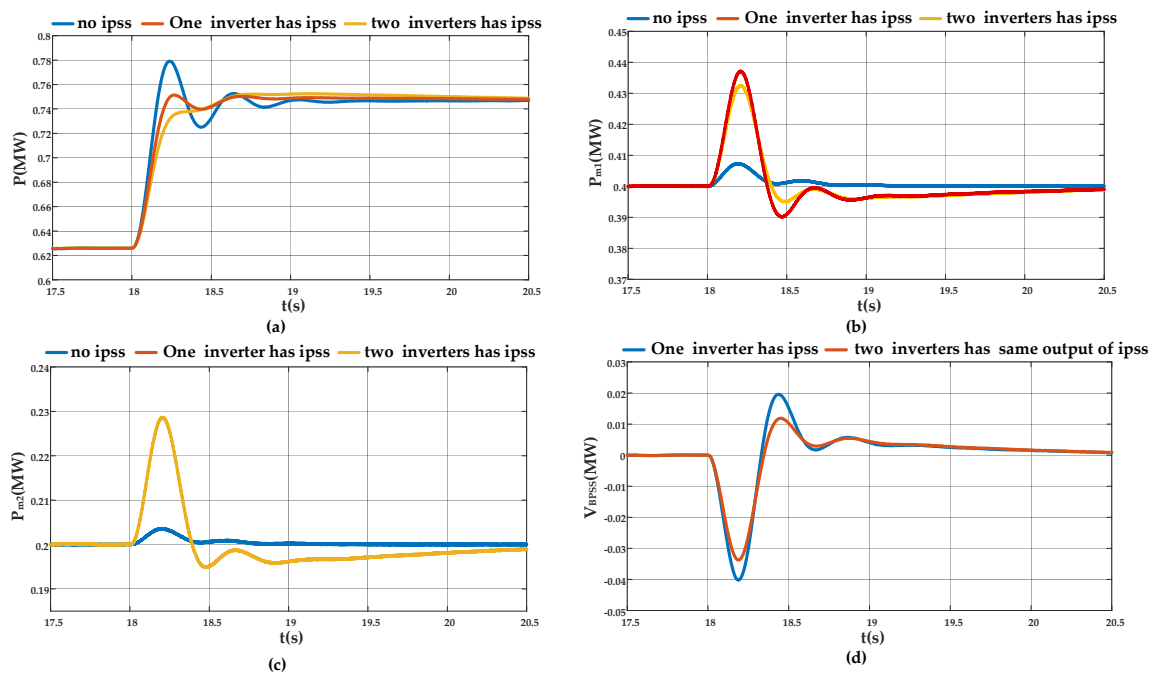


Figure 11. Simulation results of two parallel grid-connected inverters system with different built-in PSS situations, case I: none of the inverters has built-in PSS; case II: only the larger output inverter has built-in PSS; case III: both of the inverters have built-in PSS. (a) Active power fluctuation comparison of generator under the three cases; (b) active power of the larger output inverter under the three cases; (c) active power of the lower output inverter under the three cases; (d) output of built-in PSS in the inverters under the three cases.

4.5. Experimental Results

The experimental platform is consisted of one synchronous generator, two inverters and resistances. The structure of the system is same with the simulation system structure as shown in Figure 8. The experimental platform is shown in Figure 12. The parameters of the experimental platform are shown in Table 3. The two inverters all adopt same control

and built-in PSS. The excitation system and the inverters use the same control parameters as shown in Table 1.

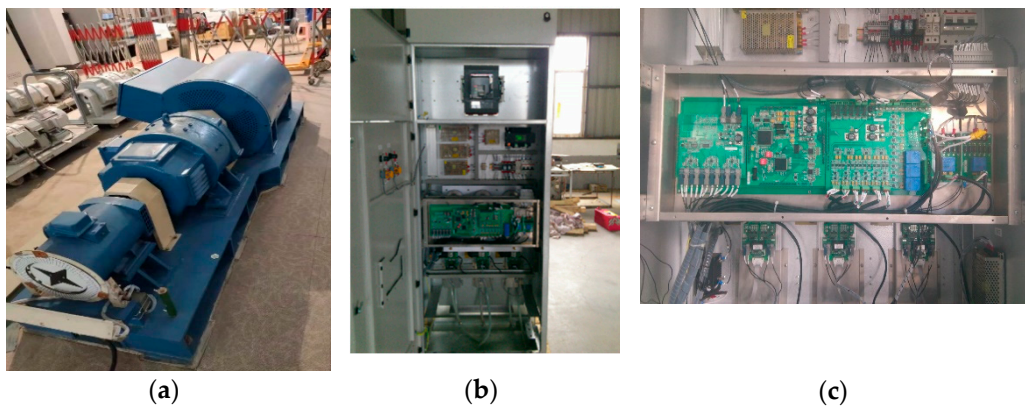


Figure 12. Experiment platform. (a) Synchronous generator; (b) inverter; (c) controller of the inverter.

Table 3. The parameters of the experimental platform.

Parameters		Values
Generator	S_{base}	30 kVA
	U_{tbase}	400 V
	x'_d	0.3556 pu
	x_q	1.0825 pu
	T'_{d0}	6.55
LCL filter	L_1	0.2 mH
	L_2	0.04 mH
	C	15 uF
load	r	2.4 Ω
DC source	V_{dc}	400 V

The parameters of built-in PSS are designed as the analysis above and shown in Table 4.

Table 4. Parameters of built-in PSS of inverter for experiment.

T_{w1}	T_{w2}	T_{w3}	T_{w4}	T_6	T_7	M
2	2	2	2	0	10	5
N	K_{s2}	K_{s3}	T_8	T_9	T_1	T_2
1	3.2	1	0.2	0.05	0.15	0.01
T_3	T_4	K_{s1}	V_{BPSS_max}	V_{BPSS_min}		
0.15	0.01	6.3	0.9 kW	−0.9 kW		

Three percent step of the generator terminal voltage test is used as the test condition. The active power waveforms of the generator under the system with and without built-in PSS are shown in Figure 13. To illustrate the damping effect of the built-in PSS with different parameters, the waveform of with built-in PSS 1 uses the parameters in Table 4 and the waveform of with built-in PSS 2 adopts the parameters in Table 4 except $T_1 = T_3 = 0.16$, $K_{s1} = 7.3$. The data of active power is recorded by controller of the inverter. The active power waveforms are obtained by using data processing software to process the recorded

data. From the comparison, the inverters with built-in PSS can increase the low frequency damping. The low frequency damping can be controlled through the adjusting of the parameters. The result is consistent with theoretical analysis above.

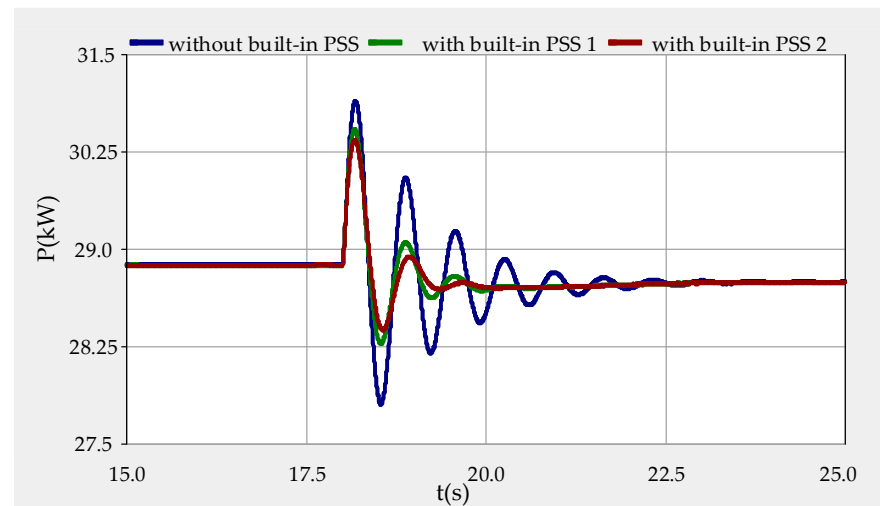


Figure 13. Active power waveform of the generator under the system with and without built-in PSS.

The oscillation information can be obtained through the input signals of the transmission active power and angular velocity. The lead-lag component compensates the phase shift caused by the power electronics-based AC grid. That makes the inverter can provide the corresponding active power variation to suppress the oscillation. The simulation and experimental result illustrate that the built-in PSS could increase low frequency damping with the proposed parameters design. The simulation and experimental results are consistent with the above theoretical analysis. The analysis is also suitable for multi parallel grid-connected inverters system in the power grid with synchronous generator characteristics.

5. Conclusions

Under the new situation that larger scale power electronics equipment and synchronous generator coexist in the power grid, making inverter participate in low frequency damping control is the key to enhancing system stability. In this paper, the low frequency damping control for power electronics-based AC power system using inverters with built-in PSS is analyzed. The model of the impact of the grid-connected inverter on the electromagnetic torque of the synchronous generator is researched and proposed. The model is the basis of increasing accurate positive low frequency damping torque through the grid-connected inverter. The built-in PSS of the inverter is used to introduce additional positive damping torque for the system. The structure of the built-in PSS is illustrated. Angular velocity and active power are used as input signals. Through lead-lag components, the built-in PSS makes inverter generate positive damping torque to increase low frequency damping. The built-in PSS control can be superposition to active power control or reactive power control loop of the inverter. The design method for the main parameter of built-in PSS is also proposed. Finally, the correctness of the theoretical analysis and the effectiveness of the built-in PSS is verified by the simulation and experiment.

Author Contributions: Conceptualization, W.C. and M.Y.; Data curation, M.Y.; Funding acquisition, J.Z.; Methodology, M.Y. and T.L.; Software, T.L.; Validation, W.L.; Writing—original draft, M.Y. and T.L.; Writing—review & editing, W.C. and M.Y. All authors have read and agreed to the published version of the manuscript.

Funding: This research was supported in part by the National Natural Science Foundation of China (Grant Number 51877042).

Institutional Review Board Statement: Not applicable.

Informed Consent Statement: Not applicable.

Data Availability Statement: Not applicable.

Conflicts of Interest: The authors declare no conflict of interest.

References

1. Chompoobutrgool, Y.; Ghandhari, M.; Vanfretti, L. Survey on power system stabilizers control and their prospective applications for power system damping using synchrophasor-based wide-area systems. *Eur. Trans. Electr. Power* **2011**, *21*, 2098–2111. [[CrossRef](#)]
2. Pogaku, N.; Prodanovic, M.; Green, T.C. Modeling, analysis and testing of autonomous operation of an inverter-based microgrid. *IEEE Trans. Power Electron.* **2007**, *22*, 613–625. [[CrossRef](#)]
3. Qi, J.; Wu, Q.; Zhang, Y.; Weng, G.; Zhou, D. Unified residue method for design of compact wide-area damping controller based on power system stabilizer. *J. Mod. Power Syst. Clean Energy* **2020**, *8*, 366–375. [[CrossRef](#)]
4. Zhong, Q.; Weiss, G. Synchronverters: Inverters that mimic synchronous generators. *IEEE Trans. Ind. Electron.* **2011**, *58*, 1259–1267. [[CrossRef](#)]
5. Alipoor, J.; Miura, Y.; Ise, T. Stability assessment and optimization methods for microgrid with multiple VSG units. *IEEE Trans. Smart Grid* **2018**, *9*, 1462–1471. [[CrossRef](#)]
6. Jiang, Q.; Li, B.; Liu, T. Large-scale power base's impact on low frequency oscillation characteristic in UHVAC power transmission system. *IEEE Access* **2019**, *7*, 56423–56430. [[CrossRef](#)]
7. Kundur, P. *Power System Stability and Control*; McGraw-Hill: New York, NY, USA, 1994.
8. Zhou, J.; Shi, P.; Gan, D.; Xu, Y.; Xin, H.; Jiang, C.; Xie, H.; Wu, T. Large-scale power system robust stability analysis based on value set approach. *IEEE Trans. Power Syst.* **2017**, *32*, 4012–4023. [[CrossRef](#)]
9. Chen, H.; Yu, W.; Liu, Z.; Yan, Q.; Tasiu, I.A.; Han, Z. Low-frequency instability induced by hopf bifurcation in a single-phase converter connected to non-ideal power grid. *IEEE Access* **2020**, *8*, 62871–62882. [[CrossRef](#)]
10. Zhou, J.; Ke, D.; Chung, C.Y.; Sun, Y. A computationally efficient method to design probabilistically robust wide-area PSSs for damping inter-area oscillations in wind-integrated power systems. *IEEE Trans. Power Syst.* **2018**, *33*, 5692–5703. [[CrossRef](#)]
11. Xiong, L.; Zhuo, F.; Wang, F.; Liu, X.; Chen, Y.; Zhu, M.; Yi, H. Static synchronous generator model: A new perspective to investigate dynamic characteristics and stability issues of grid-tied PWM inverter. *IEEE Trans Power Electron.* **2016**, *31*, 6264–6280. [[CrossRef](#)]
12. Yao, W.; Jiang, L.; Wen, J.; Wu, Q.H.; Cheng, S. Wide-area damping controller of FACTS devices for inter-area oscillations considering communication time delays. *IEEE Trans. Power Syst.* **2014**, *29*, 318–329. [[CrossRef](#)]
13. Zhang, C.; Ke, D.; Sun, Y.; Chung, C.Y.; Xu, J.; Shen, F. Coordinated supplementary damping control of DFIG and PSS to suppress inter-area oscillations with optimally controlled plant dynamics. *IEEE Trans. Sustain. Energy* **2018**, *9*, 780–791. [[CrossRef](#)]
14. D'Arco, S.; Suul, J.A. Equivalence of virtual synchronous machines and frequency-droops for converter-based microgrids. *IEEE Trans. Smart Grid.* **2014**, *5*, 394–395. [[CrossRef](#)]
15. Wen, B.; Boroyevich, D.; Burgos, R.; Mattavelli, P.; Shen, Z. Small signal stability analysis of three-phase AC systems in the presence of constant power loads based on measured D-Q frame impedances. *IEEE Trans. Power Electron.* **2015**, *30*, 5952–5963. [[CrossRef](#)]
16. Amin, M.; Molinas, M. Small-signal stability assessment of power electronics based power systems: A discussion of impedance- and eigenvalue-based methods. *IEEE Trans. Ind. Appl.* **2017**, *53*, 5014–5030. [[CrossRef](#)]
17. Wen, B.; Boroyevich, D.; Burgos, R.; Mattavelli, P.; Shen, Z. Analysis of D-Q small-signal impedance of grid-tied inverters. *IEEE Trans. Power Electron.* **2016**, *31*, 675–686. [[CrossRef](#)]
18. Ashabani, M.; Mohamed, Y.A.R.I. Mohamed. Integrating VSCs to weak grids by nonlinear power damping controller with self-synchronization capability. *IEEE Trans. Power Syst.* **2014**, *29*, 805–813. [[CrossRef](#)]
19. Kalcon, G.O.; Adam, G.P.; Anaya-Lara, O.; Lo, S.; Uhlen, K. Small-signal stability analysis of multi-terminal VSC-based DC transmission systems. *IEEE Trans. Power Syst.* **2012**, *27*, 1818–1830. [[CrossRef](#)]
20. Hassan, L.H.; Moghavvemi, M.; Almurib, H.A.; Muttaqi, K.M. A coordinated design of PSSs and UPFC-based stabilizer using genetic algorithm. *IEEE Trans. Ind. Appl.* **2014**, *50*, 2957–2966. [[CrossRef](#)]
21. Zhang, K.; Shi, Z.; Huang, Y.; Qiu, C.; Yang, S. SVC damping controller design based on novel modified fruit fly optimization algorithm. *IET Renew. Power Gener.* **2017**, *12*, 90–97. [[CrossRef](#)]
22. Zuo, J.; Li, Y.; Shi, D.; Duan, X. Simultaneous robust coordinated damping control of power system stabilizers (PSSs), static var compensator (SVC) and doubly-fed induction generator power oscillation dampers (DFIG PODs) in multi machine power systems. *Energies* **2017**, *10*, 565–588.
23. Ahmed, M.; Vahidnia, A.; Datta, M.; Meegahapola, A. An adaptive power oscillation damping controller for a hybrid AC/DC microgrid. *IEEE Access* **2020**, *8*, 69482–69495. [[CrossRef](#)]
24. Kerdphol, T.; Waranabe, M.; Hongesombut, K.; Mitani, Y. Self-adaptive virtual inertia control-based fuzzy logic to improve frequency stability of microgrid with high renewable penetration. *IEEE Access* **2019**, *7*, 76071–76083. [[CrossRef](#)]

25. Zhou, Y.; Liu, J.; Li, Y.; Gan, C.; Li, H.; Liu, Y. A gain scheduling wide-area damping controller for the efficient integration of photovoltaic plant. *IEEE Trans. Power Syst.* **2019**, *34*, 1703–1715. [[CrossRef](#)]
26. Wan, C.; Huang, M.; Tse, C.K.; Ruan, X. Effects of interaction of power converters coupled via power grid: A design-oriented study. *IEEE Trans. Power Electron.* **2015**, *30*, 3589–3600. [[CrossRef](#)]
27. Liu, J.; Miura, Y.; Ise, T. Comparison of dynamic characteristics between virtual synchronous generator and droop control in inverter based distributed generators. *IEEE Trans. Power Electron.* **2016**, *31*, 3600–3611. [[CrossRef](#)]
28. Huang, L.; Xin, H.; Wang, Z. Damping low-frequency oscillations through VSC-HVDC stations operated as virtual synchronous machines. *IEEE Trans. Power Electron.* **2018**, *34*, 5803–5818. [[CrossRef](#)]
29. Faraji, A.; Naghshbandy, A.H.; Baayeh, A.G. A hybrid coordinated design method for power system stabilizer and FACTS device based on synchro squeezed wavelet transform and stochastic subspace identification. *J. Mod. Power Syst. Clean Energy* **2020**, 1–10. [[CrossRef](#)]